analytical chemistry

pubs.acs.org/ac Article

# Diagnosis of Ischemic Renal Failure Using Surface-Enhanced Raman Spectroscopy and a Machine Learning Algorithm

Sanghwa Lee, Jeongmin Oh, Kwanhee Lee, Minju Cho, Bjorn Paulson, and Jun Ki Kim*

Cite This: *Anal. Chem.* 2022, 94, 17477−17484 Read Online

ACCESS | Metrics & More | Article Recommendations

**ABSTRACT:** To diagnose renal function using a biochip capable of detecting SERS and to assess Raman measurements taken from a bilateral renal ischemia model and the feasibility of early diagnosis was done. After generating a bilateral renal ischemia rat model, blood and urine were collected. After confirming the presence of renal injury and function, liquid drops were placed onto a Raman chip whose surface had been enhanced with Au-ZnO nanorods. SERS biomarkers that diffused into the nanogaps were selectively amplified. Raman signals varied based on the severity of the renal function, and these differences were confirmed statistically. These results confirm that renal ischemia leads to renal dysfunction and that surface-enhanced Raman spectroscopy and a machine learning algorithm can be used to track signals in the urine from the release of SERS biomarkers.

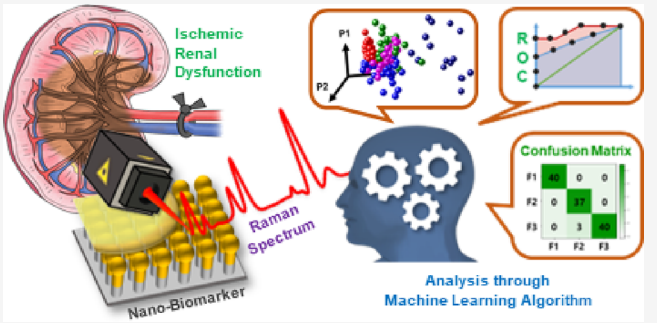


## INTRODUCTION

Acute kidney injury (AKI) refers to the clinical observation of a rapid decrease in renal function, which results in the accumulation of waste products in the serum and in the body's inability to maintain electrolyte, acidity, and water homeostasis. AKI may arise because of a variety of complex causes.[1,2] In particular, the kidney is highly sensitive to ischemia insult, and ischemia is a common cause of AKI.[2,3] In humans, acute kidney disease often presents bilaterally as blood supply leading to both kidneys is interrupted simultaneously.[4] Early diagnosis of AKI and its risk factors may enable preventative interventions, and reversal of symptoms before permanent kidney damage is sustained may prevent the development of chronic progressive kidney disease. In standard clinical practice, AKI is diagnosed according to its functional effect on glomerular filtration; high blood urea nitrogen (BUN), high serum creatinine (sCr), and a low BUN-to-creatinine ratio are biomarkers for AKI that can be detected using common commercial assays. On the basis of a rapid (within hours) increase in sCr levels and decrease in urine output, AKI severity is classified either between "Risk" and "End-stage kidney disease" on the RIFLE (Risk, Injury, Failure, Loss of kidney function, and End-stage kidney disease) criteria[5] or as one of three stages of severity in the AKIN (Acute Kidney Injury Network) criteria,[6] which have recently been revised into the KDIGO (Kidney Disease Improving Global Outcomes) criteria.[2,7]

Despite their widespread use as measures of glomerular filtration for the diagnosis of AKI, creatinine and urine outputs are lagging indicators of kidney damage, and thus they are poorly suited in the early detection of AKI.[8] In addition, sCr measurements may be confounded[9] and thus may not accurately reflect glomerular filtration rate during acute ischemia.

Depending on their size, biomarkers such as biopsy tissue (∼1 mm diameter), cells (∼tens of μm), erythrocytes (∼8 μm), bacteria (∼1 μm), viruses (∼400 nm), exosomes (several to tens of nm), proteins, or small biomolecules such as nucleic acids and cytokines are typically targeted for general diagnosis in human tissue and blood.[10−12] Various biomarkers are mixed in liquid biological byproducts such as blood or urine, and nanometer-scale markers such as small molecule targets are also included in small amounts in liquid samples. Blood that enters the kidneys through the renal artery passes through a bundle of thin capillaries called the glomerulus and secretes water, electrolytes, and various waste products into the Bowman's capsule. Large particles in the blood pass through the glomerulus, while smaller plasma components are pushed out of the glomerulus and into the Bowman capsule by osmotic pressure. Inorganic salts, amino acids, glucose, urea, and water, which have small molecular weights, are filtered, but substances with high molecular weights, such as erythrocytes, proteins,

Received: August 19, 2022
Accepted: November 28, 2022
Published: December 8, 2022







https://doi.org/10.1021/acs.analchem.2c03634
*Anal. Chem.* 2022, 94, 17477−17484

Scheme 1. Scheme of the Renal Ischemia Diagnosis Experiment Using SERS Detection and Machine Learning Algorithm[a]

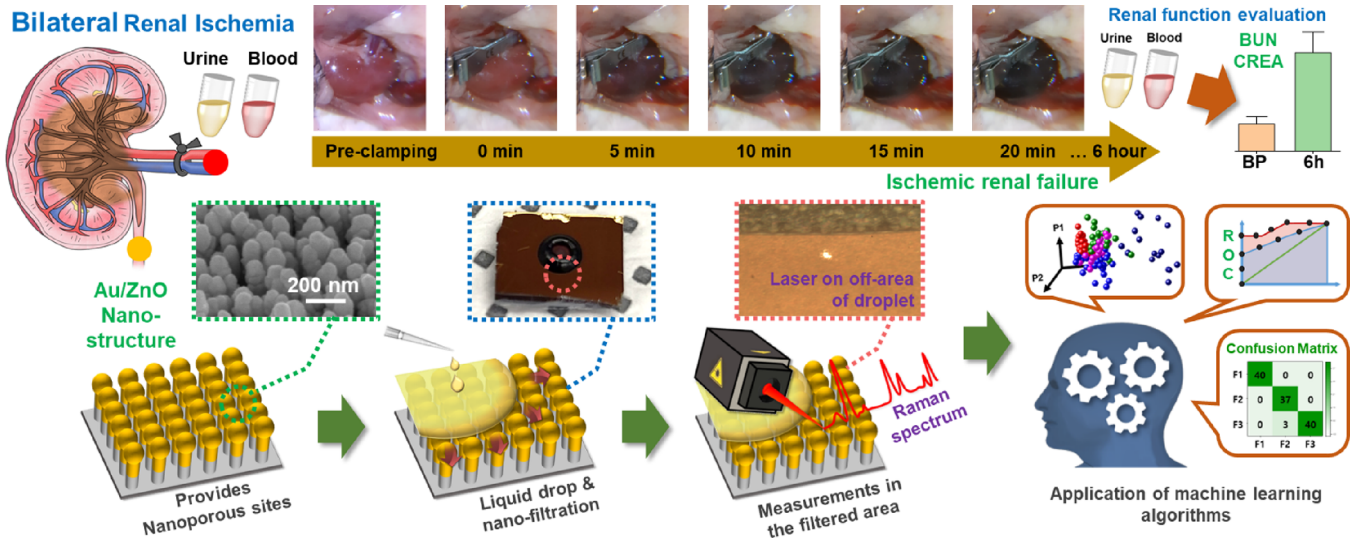


[a]BUN, blood urea nitrogen; Au-ZnO, gold-zinc oxide; BP, blood pressure, CREA, creatinine.

and fats, cannot be filtered.[3,8] Therefore, it is expected that monitoring of biomarkers in the blood will correlate with non-invasive monitoring of biomarkers in the urine, and early diagnosis of renal dysfunction may also be possible through changes in concentrations of nanometer-scale biomarkers.

Indeed, several biomarkers, including neutrophil gelatinase–associated lipocalin (NGAL), cystatin C, kidney injury molecule-1 (KIM-1), tissue inhibitor of metal-loproteinases-2 (TIMP-2), interleukin-18 (IL-18), and insulin-like growth factor-binding protein (IGFBP7), have been proposed for early detection of AKI.[8,13] In humans, these early biomarkers, especially NGAL, can be used to make diagnoses 2 to 3 days prior to those based on sCr.[14] At present, commercially available kits for the detection of NGAL biomarkers are based on chemiluminescent immunoassays, require microliters of plasma to hundreds of microliters of urine, and produce results within 15 to 35 min.[15] While suitable for clinical use, these assays are, by design, unable to detect signals of novel or unanticipated biomarkers.[15,16]

Present (optical) technologies for detection of biomarkers often require selectively separating nanometer biomarkers from the liquid sample in which biomarkers of various sizes and shapes are found, and amplification technology is required because the absolute volume of SERS biomarkers is small. Although polymerase chain reaction (PCR) technology is used for the amplification of genetic information, a technology for amplifying optical signals through surface enhancement Raman technology is emerging[17,18] and promises an approach to increase sensitivity without the primers required for PCR. In a previous study, biomarkers were selectively filtered out using a surface-enhanced Raman chip with gold-zinc oxide (Au-ZnO)-based nanometer porosity, and Raman signals were amplified using localized surface plasmon resonance.[19−21] It was confirmed that the Raman signal amplified from even a small (5 $\mu$L) droplet has high reproducibility and can be used to diagnose kidney injury from urine. In particular, in the case of kidney injury, the damage was caused by an increase in intrarenal pressure induced by ureteral obstruction, and the diagnosis basis was secured by the detection of collagen by destruction of tubular cells through surface-enhanced Raman spectroscopy (SERS).[19] However, in order to monitor a patient's health and manage AKI safely, a technology that can evaluate kidney function more sensitively and earlier is required.

Automated data analysis through artificial intelligence (AI) has been attracting attention to Raman signal analysis owing to the recent improvement in high-sensitivity signal acquisition technologies based on SERS and computer-based analysis.[22] In particular, Raman signal analyses for biological samples have significant data variance compared to those for crystalline samples, and since the biomaterials present in biological samples occupy major Raman peaks, contrast enhancement is required to detect sensitive changes. Thus, a variety of machine learning techniques have been introduced to extract meaningful diagnostic signals from SERS data.[22] Artificial intelligence methods of nonlinear classification, such as deep neural networks, support classification based on arbitrarily complex patterns and have been applied in the detection of metabolites from SERS data.[23] However, these classifiers are black boxes, and care must be taken to ensure that training data is without bias and representative of clinical samples. Other classification methods based on SERS, such as support vector machines (SVMs), which are desirable for their deterministic properties, have enabled point-of-care diagnosis in ophthalmology.[24] Although SVMs are resistant to overfitting, their application in SERS benefits from careful kernel selection.[22]

A similarly deterministic method is discriminant analysis (DA), which determines a hyperplane that minimizes the difference in data between different classes while minimizing the in-class variance.[22] While DA cannot be applied to raw Raman spectra owing to high variable collinearity and a large number of data dimensions relative to measurements, DA may be combined with other techniques, which reduce data dimensionality along the dimensions that maximize correlated variance. Principal component analysis (PCA) followed by DA has served this function in the detection of cancer,[25] and DA combined with partial least squares (PLS-DA)[26] has been observed to outperform PCA in discrimination tasks.[27] Thus,


https://doi.org/10.1021/acs.analchem.2c03634
Anal. Chem. 2022, 94, 17477−17484

research is required that derives hidden sensitivity by applying DA tools known in machine learning to Raman analysis.

In this paper, using a Au-ZnO nanostructure-based SERS chip and amplifying their signals, spectral signals were obtained to evaluate renal function from the blood and urine of bilateral renal ischemic rats. SERS-based renal function evaluation was performed through statistical processing of principal component analysis (PCA) and by using a machine learning algorithm to extract meaningful Raman signals.

## EXPERIMENTAL SECTION

**Animal Preparation and Surgical Procedure for Bilateral Renal Ischemia Models.** All animal experiments were approved by the Institutional Animal Care and Use Committee of the Asan Institute for Life Sciences, Asan Medical Center (2020-12-111), under the laws of the Republic of Korea. Six-week-old female rats (Sprague−Dawley rat, Orientbio, Korea) were used in this experiment. The rats were divided into two groups: six for the ischemic kidney model and six for the control group. The rat was anesthetized with 30 mg/kg Zoletil (Virbac, France) and 5 mg/kg Rompun (Xylazine, Bayer, Germany). The fur of the abdomen region was removed with an electric razor and hair-removal cream. The defurred abdomen was sterilized with 70% ethanol and a povidone-iodine stick. Urine and blood samples were collected before surgery. The urine sample was collected by gently applying pressure to the lower abdomen. Blood samples were drawn from the tail vein. After the sample collection, the operator opened up the abdominal cavity. For the control group, the abdominal cavity was closed with 5−0 suture thread (Ethilon, USA). For the ischemic renal group, both kidneys were exposed and ligated with suture thread. Ligation was confirmed with visual examination of the color of the kidneys as shown in Scheme 1. The abdominal cavity was closed with suture thread, and the rats were left free in the cage for 6 h. After 6 h, blood and urine samples were collected using the same method with pre-ligation. The sutured abdominal cavity was re-opened, and the ligated kidney was freed by removing the suture thread. Perfusion of blood was performed by injecting phosphate-buffered saline to the heart. The rat was euthanized in deep anesthesia as perfusion drew blood out of the system.

**Hematoxylin−Eosin Staining for the Kidney Damage Evaluation.** Bilateral kidneys were collected from normal and ligated kidney rats and then fixed in 4% buffered paraformaldehyde for 24 h. The paraformaldehyde-fixed kidneys were aspirated, embedded in a paraffin block, and sliced into a 3 $\mu$m thickness for staining. The slice was stained with hematoxylin−eosin (H&E) for the morphological evaluation of the injury. Stained H&E slides were analyzed on a microscope (Olympus CKX41, Japan), and images were taken at 20× and 40× magnification with a digital camera (Olympus DP73, Japan) and Cellsens software (Olympus, Japan).

**Postsurgical Procedure for the Collection of Blood and Urine Samples.** The collected whole blood samples were allowed to clot at room temperature for 30 min and centrifuged at 3000 rpm for 10 min, and the upper serum was separated. Blood urea nitrogen (BUN) was analyzed from serum with a clinical analyzer (HITACHI Clinical Analyzer 7180, Japan). Fresh urine was immediately taken for the creatinine level evaluation. Serum and urine creatinine were also analyzed with the clinical analyzer (HITACHI Clinical Analyzer 7180, Japan).

**Synthesis of ZnO Nanostructures and the Deposition of Au.** To amplify the Raman signals *via* the SERS substrate, vertically aligned ZnO nanorods were grown using hydrothermal synthesis as a nanostructural framework. The synthesis solution for the ZnO nanostructure was prepared by dissolving 10 mM zinc nitrate hexahydrate (Sigma Aldrich Co., St. Louis, USA) and 0.9 mL of ammonium hydroxide (Sigma Aldrich Co., St. Louis, USA) in 30 mL of deionized water. The silicon (Si) wafer (LG SILTRON INC., Korea) was then immersed in the aqueous solution for 50 min in an oven set to 90 °C. The grown nanorods on Si substrates were 400−600 nm in length and 50 nm in diameter. A 200 nm thickness of Au was coated on ZnO nanorods using a thermal evaporator (Alpha Plus Co., Korea), and the morphology of the nanostructure was analyzed by a field-emission scanning electron microscope (FE-SEM, S-4700, HITACHI, Japan).

**Raman Spectrum Acquisition and Post-signal Processing.** The urine and blood drops are delivered to the SERS chip in their raw form, without incubation or pretreatment, and are stored in a clean bench environment at approximately 25 °C. The 5 $\mu$L drops of serum and urine obtained from bilateral renal ischemic animals were placed on a SERS chip and left for 30 min to allow the biomarkers time to infiltrate the nanocavities of the SERS chip.

The chips were then loaded into a microscope (IX-73, Olympus, Japan) and analyzed using a Raman spectroscopy system (FEX-INV, NOST, Korea) with a 785 nm diode laser as the excitation source attached to the microscope. As in Scheme 1, after confirming the droplet boundary with a microscope during Raman measurement, the laser point position was checked within a distance of 50 $\mu$m to obtain a Raman signal. The droplet interface was confirmed with an image through a 40× objective lens (LUCPLFLN, OLYMPUS, Japan), and a Raman signal was obtained using a 1.2 mW laser power and a 100× objective lens (UPLXAPO, OLYMPUS, Japan). For spike removal and noise removal, a single spectrum was obtained by accumulating for 10 s each. The Raman spectra ranged from 450 to 2450 $cm^{-1}$, with a spectral resolution of 1 $cm^{-1}$. By measuring 10 points on each rat, Raman signals were analyzed using 40 points per case. The measured raw Raman spectrum was post-processed through 3rd-order polynomial fitting to remove background noise and smoothed using the Savitzky−Golay method. Assignment to the peaks of the post-processed signal was performed as shown in Table 1.

**Statistical Analysis and Application of Machine Learning Algorithms to Raman Spectral Data.** PCA was introduced for dimensionality reduction and statistical analysis of the value variable according to the identity of the Raman spectrum, peaks, or energy shift. The entire spectral range was used as a variable, consisting of 2000 points from 450 to 2450 $cm^{-1}$ with a 1 $cm^{-1}$ step. To secure Raman spectroscopy-based diagnostic criteria, partial least squares (PLS)-based DA, one of the machine learning algorithms, is applied. From the PLS-DA application, the data score distribution and confusion matrix in normal and ischemic animal models were confirmed. Receiver operating characteristic (ROC) curves were obtained by measuring sensitivity and specificity in blood and urine, respectively, and the diagnosis rate was obtained from the area under the ROC curve (AUC). The PCA and PLS-DA were conducted using XLSTAT 2019 software.



https://doi.org/10.1021/acs.analchem.2c03634
Anal. Chem. 2022, 94, 17477−17484

Table 1. Assignments of Peaks Observed in Raman Spectra

| peak ($cm^{-1}$) | assignment |
|---|---|
| 490 | glycogen[34,35] |
| 530 | S−S disulfide stretch in proteins[34,36] |
| 583 | amide-VI in serum[37,38] |
| 622 | C−C twisting mode of phenylalanine[34,36] |
| 650 | C−C twisting mode of tyrosine[37,38] |
| 712 | hypoxanthine in serum[38,39] |
| 790 | U, T, C (ring breathing modes in the DNA/RNA bases)[36,40] |
| 835 | tyrosine[36,40] |
| 890−930 | glycogen and C−C stretching of glucose[36,41] |
| 1000 | symmetric ring breathing of phenylalanine[19,21,36] |
| 1030 | C−H bending of phenylalanine[19,21,36] |
| 1140 | C−N stretching in D-mannose[35,39] |
| 1200−1350 | C−N stretching and N−H bending of amide III[40,42] |
| 1365 | tryptophan[35,36] |
| 1445 | $CH_3$, $CH_2$ bending (lipids/cholesterol/proteins)[35,43] |
| 1560 | tryptophan[35,36] |
| 1600 | C═C bending of phenylalanine[36,39] |
| 2120, 2170 | CN stretching related vibration[44,45] |

## RESULTS AND DISCUSSION

**Validation of Bilateral Renal Ischemia and Kidney Dysfunction.** To induce renal ischemic failure with uremia, bilateral renal vascular ligation was performed.[28] A model of acute renal failure was induced by renal ischemia in Sprague−Dawley rats, as shown in Scheme 1. In the case of kidney ligation, darkening due to ischemia was observed as shown in Scheme 1. The blood vessels leading to the kidneys were ligated for 6 h, with blood and urine samples collected before and after ligation, and the kidneys were observed by histology. BUN and creatinine values were measured in blood and urine, and renal function performance was confirmed by comparing the values in urine and blood obtained from the same rat before ligation. Based on this, histopathology and biochemical examination for Raman signal results and a machine learning algorithm-based analysis were prepared.

As shown in Figure 1, ligation resulted in 200 $\mu$m diameter pathologies observed under H&E-stained histology in both left and right cortices and medulla, when compared to a non-ligated control. As in other bilateral ischemia animal models,[29,30] global hemorrhage is seen in the cortex and medulla in red in ischemic animals, unlike in normal. Even though saline was used to perfuse the tissue during the acquisition process, red blood cells were trapped around the glomerulus and between the tubule cells. These red blood cells gave the H&E slide a strong red color. Furthermore, while congestion (black arrows) appears locally in Figure 1b,[31] there were no remaining red blood cells in the tissue in the case of the normal group. The tissue image shows that the blood vessels in both the left and right kidney were well ligated. This caused kidney damage due to ischemia, which shows that the kidney function was blocked during the blood and urine acquisition process.

Concomitant renal dysfunction was confirmed by observation of BUN and blood creatinine concentrations, which both increased significantly over the period of ligation. In other studies, the values of BUN and creatinine in normal rat serum were 15−21 and 0.2−0.8 mg/dL, respectively.[32,33] The average levels of BUN and sCr before ligation in Figure 1e were 18.2 ± 2.7 and 0.47 ± 0.03, respectively, and well-distributed within the normal range. These values were 52.2 ± 6.7 and 1.11 ± 0.15, respectively, after 6 h of ligation. As such, the serum urea and creatinine levels show a dramatic increase, and the results are similar to the absolute and change values in other bilateral renal injury animal models. As shown in Figure 1f, the urine creatinine level slightly increased from 7.7 ± 2.7 to 9.4 ± 3.2. This is a significantly lower change (1.2 ± 0.1 times) than the increase rate of sCr by more than two times (2.4 ± 0.3 times). With this numerical change, it is difficult to evaluate kidney function using the level of creatinine in the urine alone.

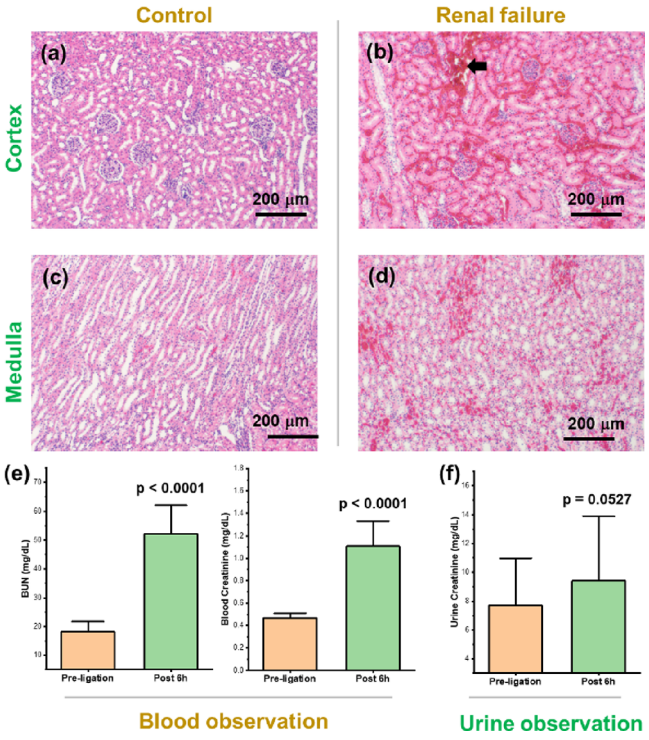


Figure 1. Evaluation of renal ischemia model production and confirmation of renal function changes. (a, c) H&E staining of the cortex and medulla of normal rats, and (b, d) left tissue images of bilateral renal ischemia animals. (e) Measurements of BUN and creatinine in rat serum before and after blood vessel ligation. (f) Creatinine measurement in urine. Black arrows indicate congestion. H&E, hematoxylin and eosin; BUN, blood urea nitrogen.

**Surface-Enhanced Raman Spectra Acquisition and Peak Assignment.** Single drops of blood and urine collected from the renal ischemia model were deposited onto Au-ZnO nanoparticle-coated Si chips, and the resultant Raman spectra were measured under illumination at 785 nm, as shown in Figure 2. For amplifying Raman signal, a skeletal structure providing nano-porous was made by growing ZnO nanorods. The gold was coated on the ZnO nanorods as a metal medium that can enhance surface plasmon resonance during the Raman signal acquisition process (Scheme 1 shows an electron microscope image). Au-ZnO nanostructures provide tens of nanometers of porosity, and blood and urine dropped on these SERS chips diffuse into the porous structure. When the diffused area is checked through a microscope, the laser is positioned, and a spectral signal is acquired; an enhanced Raman signal is acquired through plasmon resonance on the surface of the SERS biomarkers and gold nanoparticles. The average spectrum of the enhanced Raman signal was measured in blood and urine (the thick line is the average, the same color shade is the standard deviation). This is the result of measuring 40 points on test samples from four animals (Figure 2).


https://doi.org/10.1021/acs.analchem.2c03634
Anal. Chem. 2022, 94, 17477−17484

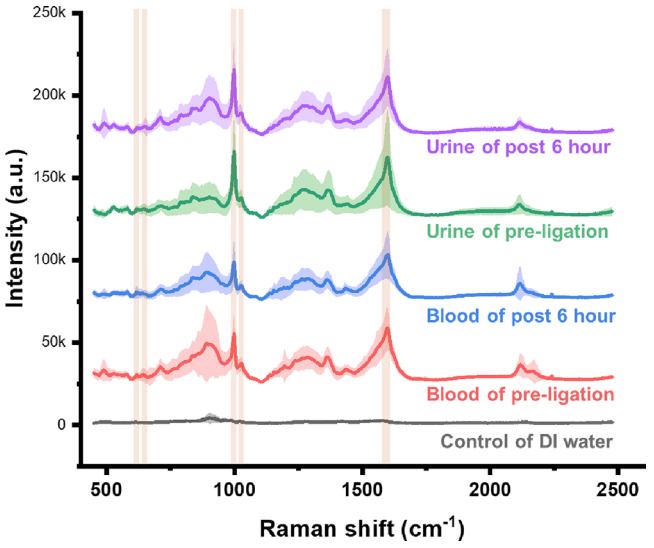


**Figure 2.** Average Raman spectra for the bilateral renal ischemia model. The standard deviation is represented by the shaded area around the solid line. Table 1 indicates mainly assigned peaks, and brown bars indicate peaks related to phenylalanine and tyrosine.

Many notable peaks in the observed Raman shifts were identified, and they are depicted as bars in Figure 2 with their corresponding vibrational modes in Table 1. A peak was assigned to SERS biomarkers such as amino acids of phenylalanine (Phe) and tyrosine (Tyr), nucleic acids, and proteins. Most notably, symmetric ring breathing and C−H bending corresponding to Phe were observed at 1000 and 1030 $cm^{-1}$, respectively. Plasma Phe is a known marker of renal failure, as the metabolism of Tyr depends on kidney function.[46,47] The related peaks are separately indicated by brown bars in Figure 2, but it is also difficult to determine the diagnostic potential through visual graphs. In this study, the Raman spectrum consists of the peaks from different markers and the peaks from the amino acids listed above. In order to secure the diagnostic performance and evidence of the Raman spectrum obtained from the bilateral renal ischemia model, the characteristics for each data point were determined by setting the peak of the entire spectrum as a variable.

**PCA of Raman Spectra for Liver Function Evaluation.** An initial PCA was performed on the observed Raman spectra to reveal the orthogonal principal components (PCs) of the spectrum that most efficiently capture the correlated spectral variance between measurements. For example, the first PC (PC1) captures the largest variance, the second PC (PC2) captures the second-largest variance, and so on. The Raman spectra for each measurement were then decomposed into the amplitudes of their PCs and graphed in PC space. Graphing each observation by its PCs often allows data to be easily clustered and thus categorized by diagnosis. As depicted in Figure 3, when PCs were calculated over the full dataset, the Raman spectra of the pre- and post-ligation blood and urine samples were not clearly separated in the PC space of the first three principal components, despite the first PC accounting for 63% of the variability in the data, the second PC accounting for 9% of the variability in the measurements, and the third PC accounting for 4% of the variability. The variability from PC1 to 50 is shown as a diagram in Figure 3b, and the variability with the meaning of the distance that separates data in PC space is dominated by the previous few values. Grouping was

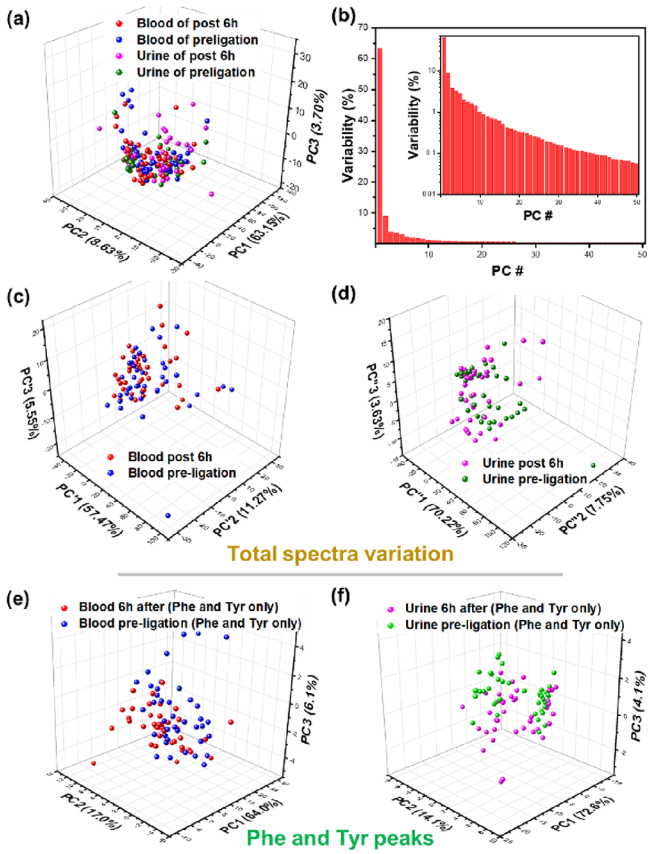


**Figure 3.** (a) Principal component analysis of the pre- and post-renal ligation Raman spectra captures sample variability but does not adequately segment it by ligation status. (b) Variability of units up to PC 50; inset is the log scale. (c, d) PCA of Raman spectra in blood and urine, respectively. (e, f) PCA of blood and urine calculated only from extracted Phe and Tyr Raman peak values. PCA, principal component analysis; Phe, phenylalanine; Tyr, tyrosine.

slightly improved but still poor when PC was calculated for blood and urine samples independently, as shown in Figure 3c,d.

Figure 3e,f shows the results of PCA by extracting the peak data for Phe and Tyr from blood and urine. These results reflects the aforementioned correlation between renal function and amino acid. There was also no data separation in PCA as there was no visible difference.

**Applying Machine Learning Algorithms for Liver Function Evaluation.** PLS-DA is a technique that generalizes PLS regression to the case of discrete classes for supervised clustering[26] and is known to outperform PCA in discrimination tasks requiring reduction of dimensions.[27] For AI-based automated diagnosis, it is necessary to increase the clarity of the diagnostic basis from a lot of data through machine learning, and the efficiency of diagnosis depends on the data separation algorithm applied. In the biomedical field, analysis of Raman signals has been analyzed with various machine learning algorithms,[22] and in this study, the diagnostic performance for machine learning was optimized through PCA-PLS analysis.

For PLS-DA, the application of Raman signal data in Figure 2 is based on 2000 variations in the range of 450 to 2450 $cm^{-1}$ (with a spectral resolution of 1 $cm^{-1}$). If 2000 variables for a single data point are measured at '$m$' points for '$n$' animals, the PLS-DA for 2000 × $n$ × $m$ is applied. If machine learning is


https://doi.org/10.1021/acs.analchem.2c03634
Anal. Chem. 2022, 94, 17477−17484

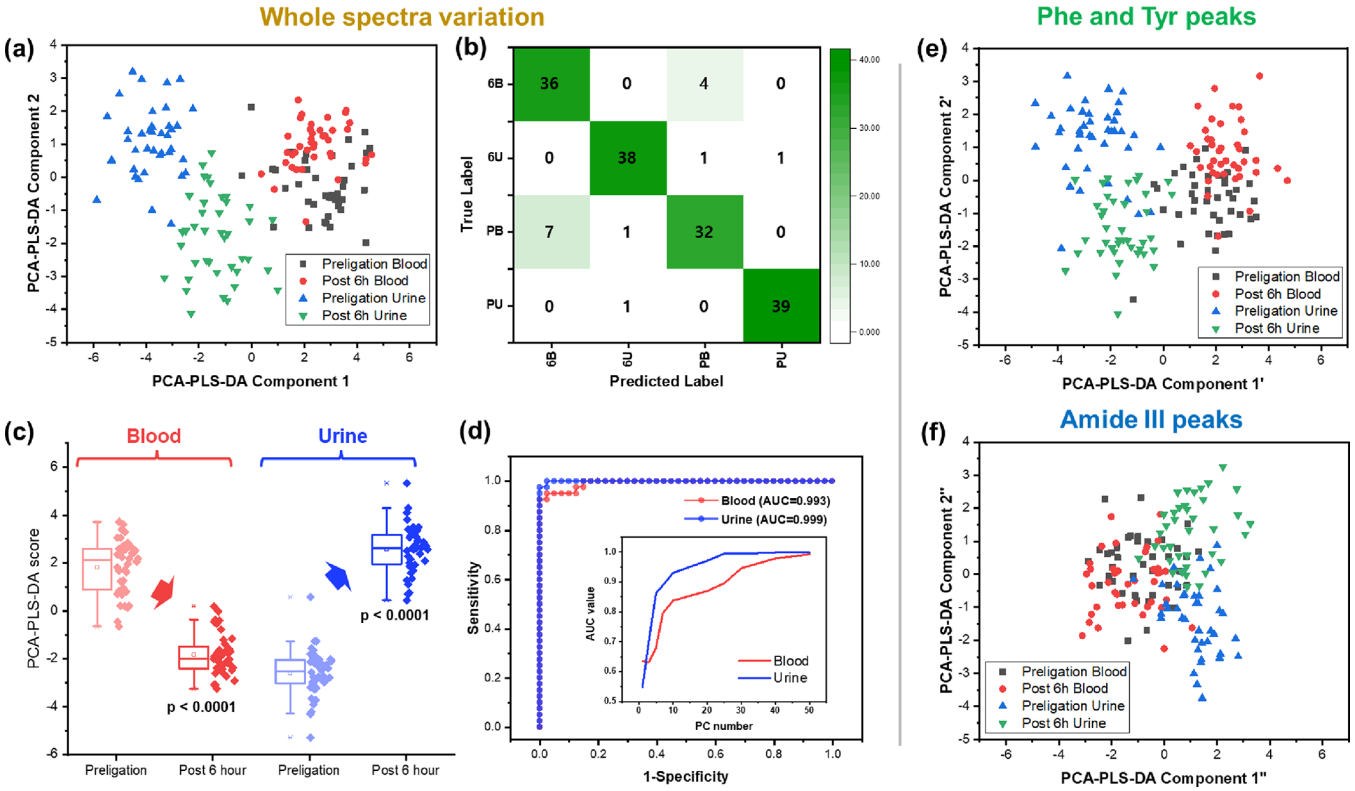


**Figure 4.** Evidence of kidney function evaluation through the use of a machine learning algorithm of PCA-PLS-DA. (a) Whole data distribution in PCA-PLS-DA1 and 2 planes and (b) confusion matrix. (c) Data distribution at the boundary of blood and urine, separately, using the same machine learning algorithm, and (d) ROC curve and AUC value for separated data in urine and blood. Inset in panel (d) is the AUC value change according to the number of PCs included in PLS-DA. PCA-PLS-DA plane images based on spectral data corresponding to (e) Phe and Tyr peaks and (f) amide III, respectively. PCA, principal component analysis; PLS, partial least squares; DA, discriminant analysis; ROC, receiver operating characteristic; AUC, area under the ROC curve; Phe, phenylalanine; Tyr, tyrosine.

performed while increasing $n$ and $m$, it takes up a lot of computer resources. In this study, after dimensional reduction through PCA, PLS-DA was implemented with the PC score as a variation. Among the PC values, the top 50 of variability were analyzed as variables, and the weight of the PC values is well shown in Figure 3b.

Applying PCA-PLS-DA as shown in Figure 4a,b, segmentation between preclinical samples was noticeably improved, and the resulting classification was highly predictive of ischemic renal function, as shown in Figure 4. In particular, pre- and post-ligation urine samples were clearly distinguishable *via* just the first two components, and the distribution and confusion matrix showed 91% of samples correctly classified with a false-positive rate of 9.7% and a false-negative rate of 7.8%, or a sensitivity of 93% and specificity of 89%. As shown in Figure 4a, in the data projected onto the PCA-PLS-DA1 and 2 planes, the data from the blood of pre- and post-ligation samples are superimposed. This is diagrammed in an optimized direction when there are four discriminant boundaries, and when PLS-DA is applied to separate blood and urine, separation is achieved as shown in Figure 4c. The blood PCA-PLS-DA scores were observed to drop during induced ischemic renal dysfunction with overlap in the error bounds, while the urinary PCA-PLS-DA scores rose enough for the two samples to not be overlapped, with 99.3% AUC for blood and 99.9% AUC for urinary assays. Optimization of the AUC value obtained through PCA-PLS-DA is dependent on the number of PC datasets included in the PLS-DA. The inset in Figure 4d shows the AUC value output according to the number of PCs included, and we confirmed that both blood and urine converge to the optimized value of 50.

Since urine and blood are collected separately during the sampling process, the value obtained from these separated AUCs is close to a direct measure of renal function. Nevertheless, the following trends were confirmed by analyzing Raman data of biomarkers in urine and blood together, as shown in Figure 4a,b. The data points in the PCA-PLS-DA space of Figure 4a show that blood and urine were well-separated in the case of pre-ligation, but they tended to approach each other after kidney injury. Considering the circumstances, such as the kidney's function to filter waste products from the blood into urine and the occurrence of hematuria owing to kidney dysfunction, the trend towards a closer approximation of these data clearly demonstrates a decline in renal function. Since there is a correlation between renal function and Phe and Tyr metabolism, statistical analysis was performed on the peak region related to the amino acid as shown in Figure 4e. For analysis and contrast of Phe and Tyr using a machine learning algorithm, the data distribution corresponding to amide III is shown in Figure 4f. The spectral peak centers of Phe and Tyr were located at 622, 650, 1000, 1030, and 1600, and the range corresponding to $\pm 10$ cm$^{-1}$ of each peak was designated as a variable for statistical analysis. Amide III was assigned a range of 1200−1350 cm$^{-1}$ as a variable for statistical analysis, and peaks corresponding to Phe, Try, and Amide III are underlined in Table 1. Comparing Figure 4e and 4f, Phe and Tyr signals have a large contribution to the Raman analysis for the evaluation of renal function.


https://doi.org/10.1021/acs.analchem.2c03634
Anal. Chem. 2022, 94, 17477−17484

Values corresponding to the spectral region that was analyzed selectively may be contributed by other biomaterials in blood and urine other than Phe and Tyr. Based on the correlation between renal function and Phe/Tyr metabolism and the contribution of Raman data, the evaluation of the renal function of biomarkers through SERS is reasonable. Additionally, using machine learning algorithms to analyze the entire spectrum region allows for more accurate diagnostic criteria to be found from a wider range of factors.

While not directly comparable due to the preclinical nature and the different timing of these assays, the sensitivity and specificity obtained compare favorably to some AKI assays developed based on other known kidney biomarkers, such as the 2 h urine NGAL immunofluorescent assay, which showed sensitivity of 0.82 and specificity of 0.90 for prediction of AKI in small clinical trials ($N = 100$),[48,49] or the serum cystatin C-based assay, which showed clinical sensitivity and specificity of 0.86 and 0.82, respectively.[50] Unlike previous AKI assays, the present sensing chip does not target a specific known biomarker and thus has the potential to be more accurate and more predictive than assays based on single biomarkers. However, machine learning techniques are of limited applicability beyond their training regime, and so clinical translation of the present SERS- and machine learning-based techniques for early diagnosis of AKI depends on collecting a wide variety of samples for calibration and training. Future studies are required to examine the clinical relevance by accumulating data through extension to animal models with unilateral kidney injury animal models and application to renal disease samples from patients.

## CONCLUSIONS

In summary, surface-enhanced Raman signals for biomarkers were obtained from blood and urine for renal function evaluation, and Raman signals were classified according to function using a machine learning algorithm. Blood and urine samples were collected from rat animals with bilateral ischemia and renal dysfunction. The kidneys were removed, histopathological analysis was performed, and it was confirmed that the injury had developed in bilateral kidneys. BUN in serum was measured, and sCr and urine creatinine were detected to evaluate kidney function standards. For the detection of SERS, a Au-ZnO-based SERS sensing chip having a nanoporous structure was prepared. When blood and urine were dropped and diffused into the nanoporous structure, and the Raman signal was enhanced. It was confirmed that the peaks of the Raman signal were derived from various biomaterials, including Phe and Tyr. Data distribution and diagnostic availability were reviewed through PCA for Raman signals, but data were not separated. It was confirmed that renal function evaluation was possible by grafting the PLS-DA mechanism, one of the machine learning algorithms. Furthermore, when measuring the renal function evaluation rate in blood and urine, respectively, it showed an accuracy of 99.3% and 99.9%.

By utilizing Raman signal enhancement with the passive characteristics of the SERS chip, we monitored and diagnosed kidney function. Using the machine learning analysis algorithms of PCA and PLS-DA, we confirmed that SERS biomarkers in blood and urine can be used as diagnostic criteria for kidney function. Phe and Tyr, unlike Amide III, were confirmed to be factors that can be used to evaluate renal function, but the accuracy was improved by using a larger Raman signal region. Signal enhancement sensing of nanoporous structures and the application of machine learning algorithms are useful for evaluating kidney function that requires multicomplex detection of various biomarkers.

## AUTHOR INFORMATION


### Corresponding Author

**Jun Ki Kim** − *Department of Convergence Medicine, University of Ulsan College of Medicine, Seoul 05505, Republic of Korea;* orcid.org/0000-0002-0099-9681; Email: kim@amc.seoul.kr

### Authors

**Sanghwa Lee** − *Biomedical Engineering Research Center, Asan Medical Center, Seoul 05505, Republic of Korea*

**Jeongmin Oh** − *Department of Convergence Medicine, University of Ulsan College of Medicine, Seoul 05505, Republic of Korea*

**Kwanhee Lee** − *Department of Convergence Medicine, University of Ulsan College of Medicine, Seoul 05505, Republic of Korea*

**Minju Cho** − *Department of Convergence Medicine, University of Ulsan College of Medicine, Seoul 05505, Republic of Korea*

**Bjorn Paulson** − *Biomedical Engineering Research Center, Asan Medical Center, Seoul 05505, Republic of Korea*

Complete contact information is available at: https://pubs.acs.org/10.1021/acs.analchem.2c03634


### Notes

The authors declare the following competing financial interest(s): J.K.K. is a scientific advisor to the startup Apollon Inc. (Korea), which may develop diagnostic devices based on this work. The authors have declared that no other competing interests exist.

## ACKNOWLEDGMENTS

This work was supported by the National Research Foundation of Korea (NRF) (2018R1D1A1B07048562, 2019R1A2C2084122, 2020R1A2C2102137) and MRC grant (2018R1A5A2020732) by the Ministry of Science and ICT (MSIT), by a grant from the Ministry of Trade, Industry, and Energy under the Industrial Technology Innovation Program (20000843), and by the Korea Health Technology R&D Project through the Korea Health Industry Development Institute (KHIDI), funded by the Ministry of Health & Welfare, Republic of Korea (HI22C1374).

## REFERENCES


(1) Togel, F.; Westenfelder, C. *F1000Prime Rep.* **2014**, *6*, 83.
(2) Makris, K.; Spanou, L. *Clin. Biochem. Rev.* **2016**, *37*, 85−98.
(3) Bonventre, J. V.; Yang, L. *J. Clin. Invest.* **2011**, *121*, 4210−4221.
(4) Wei, Q.; Dong, Z. *Am. J. Physiol. Renal.* **2012**, *303*, F1487−F1494.
(5) Bellomo, R.; Ronco, C.; Kellum, J. A.; Mehta, R. L.; Palevsky, P.; Workgroup, A. *Crit. Care* **2004**, *8*, R204−R212.
(6) Mehta, R. L.; Kellum, J. A.; Shah, S. V.; Molitoris, B. A.; Ronco, C.; Warnock, D. G.; Levin, A.; Acute Kidney Injury Network. *Crit. Care* **2007**, *11*, R31.
(7) Brar, J.; Zachariah, M.; Arora, P.; Chang, S.; Venuto, R.; Gudleski, G. *Am. J. Transplant.* **2012**, *12*, 492−492.
(8) Parikh, C. R.; Devarajan, P. *Crit Care Med* **2008**, *36*, S159−S165.
(9) Hewitt, S. M.; Dear, J.; Star, R. A. *J. Am. Soc. Nephrol.* **2004**, *15*, 1677−1689.

(10) Durand, F.; Francoz, C.; Asrani, S. K.; Khemichian, S.; Pham, T. A.; Sung, R. S.; Genyk, Y. S.; Nadim, M. K. *Transplantation* **2018**, *102*, 1636−1649.
(11) Citores, M. J.; Lucena, J. L.; de la Fuente, S.; Cuervas-Mons, V. *World J. Hepatol.* **2019**, *11*, 50−64.
(12) Lewandowska, L.; Małyszko, J.; Joanna Matuszkiewicz-Rowińska, J. *Ann. Transplant.* **2019**, *24*, 291−297.
(13) Wasung, M. E.; Chawla, L. S.; Madero, M. *Clin. Chim. Acta* **2015**, *438*, 350−357.
(14) Soni, S. S.; Ronco, C.; Katz, N.; Cruz, D. N. *Blood Purificat.* **2009**, *28*, 165−174.
(15) Soni, S. S.; Cruz, D.; Bobek, I.; Chionh, C. Y.; Nalesso, F.; Lentini, P.; de Cal, M.; Corradi, V.; Virzi, G.; Ronco, C. *Int Urol Nephrol* **2010**, *42*, 141−150.
(16) Grenier, F. C.; Ali, S.; Syed, H.; Workman, R.; Martens, F.; Liao, M.; Wang, Y.; Wong, P. Y. *Clin. Biochem.* **2010**, *43*, 615−620.
(17) Guselnikova, O.; Lim, H.; Kim, H. J.; Kim, S. H.; Gorbunova, A.; Eguchi, M.; Postnikov, P.; Nakanishi, T.; Asahi, T.; Na, J.; Yamauchi, Y. *Small* **2022**, *18*, 2107182.
(18) Huang, X.; Mahmudul, H. M.; Li, Z. B.; Deng, X. J.; Su, X. Z.; Xiao, Z. Q.; Zhao, L. Y.; Liu, T.; Li, H. Y. *Front. Biosci. Landmark* **2022**, *27*, 040.
(19) Lee, S.; Namgoong, J. M.; Jue, M.; Joung, Y.; Ryu, C. M.; Shin, D. M.; Choo, M. S.; Kim, J. K. *Int. J. Nanomed.* **2020**, *15*, 8121−8130.
(20) Lee, S.; Tak, E.; Cho, Y. J.; Kim, J.; Lee, J.; Lee, R.; Lee, K.; Kwon, M.; Yoon, Y. I.; Lee, S. G.; Namgoong, J. M.; Kim, J. K. *BioChip J.* **2022**, *16*, 49−57.
(21) Lee, S.; Namgoong, J. M.; Yu, H. Y.; Jue, M.; Kim, G.; Jeon, S.; Shin, D. M.; Choo, M. S.; Joo, J.; Pack, C. G.; Kim, J. K. *Nanomaterials* **2019**, *9*, 224.
(22) Lussier, F.; Thibault, V.; Charron, B.; Wallace, G. Q.; Masson, J. F. *TraC-Trend. Anal. Chem.* **2020**, 124.
(23) Lussier, F.; Missirlis, D.; Spatz, J. P.; Masson, J. F. *ACS Nano* **2019**, *13*, 1403−1411.
(24) Kim, W.; Lee, S. H.; Kim, S. H.; Lee, J. C.; Moon, S. W.; Yu, J. S.; Choi, S. *ACS Appl. Mater. Interfaces* **2017**, *9*, 5891−5899.
(25) Del Mistro, G.; Cervo, S.; Mansutti, E.; Spizzo, R.; Colombatti, A.; Belmonte, P.; Zucconelli, R.; Steffan, A.; Sergo, V.; Bonifacio, A. *Anal. Bioanal. Chem.* **2015**, *407*, 3271−3275.
(26) Lee, L. C.; Liong, C. Y.; Jemain, A. A. *Analyst* **2018**, *143*, 3526−3539.
(27) Barker, M.; Rayens, W. *J. Chemom.* **2003**, *17*, 166−173.
(28) Karimi, Z.; Ketabchi, F.; Alebrahimdehkordi, N.; Fatemikia, H.; Owji, S. M.; Moosavi, S. M. S. *Renal Failure* **2016**, *38*, 1503−1515.
(29) Shang, Y.; Hewage, S. M.; Wijerathne, C. U. B.; Siow, Y. L.; Isaak, C. K.; Karmin, O. *Front. Med. Lausanne* **2020**, 7.
(30) Chavez, R.; Fraser, D. J.; Bowen, T.; Jenkins, R. H.; Nesargikar, P.; Pino-Chavez, G.; Khalid, U. *J. Histol. Histopathol.* **2016**, *3*, 1−7.
(31) Koc, K.; Geyikoglu, F.; Cakmak, O.; Koca, A.; Kutlu, Z.; Aysin, F.; Yilmaz, A.; Askin, H. *Naunyn-Schmiedeberg's Arch. Pharmacol.* **2021**, *394*, 469−479.
(32) McClure, D. E. *Vet. Clin. North Am. Exot. Anim. Pract.* **1999**, *2*, 565−590.
(33) Ecelbarger, C. A.; Sands, J. M.; Doran, J. J.; Cacini, W.; Kishore, B. K. *Kidney Int.* **2001**, *60*, 2274−2282.
(34) Stone, N.; Kendall, C.; Shepherd, N.; Crow, P.; Barr, H. *J. Raman. Spectrosc.* **2002**, *33*, 564−573.
(35) Chen, N.; Rong, M.; Shao, X. G.; Zhang, H.; Liu, S. P.; Dong, B. J.; Xue, W.; Wang, T. Y.; Li, T. H.; Pan, J. H. *Int. J. Nanomed.* **2017**, *12*, 5399−5407.
(36) Talari, A. C. S.; Movasaghi, Z.; Rehman, S.; Rehman, I. U. *Appl. Spectrosc. Rev.* **2015**, *50*, 46−111.
(37) Lin, D.; Feng, S. Y.; Pan, J. J.; Chen, Y. P.; Lin, J. Q.; Chen, G. N.; Xie, S. S.; Zeng, H. S.; Chen, R. *Opt. Express* **2011**, *19*, 13565−13577.
(38) Guo, L.; Li, Y. P.; Huang, F. R.; Dong, J.; Li, F. C.; Yang, X. H.; Zhu, S. Q.; Yang, M. X. *J. Innov. Opt. Heal Sci.* **2019**, *12*, 1950003.
(39) Tan, Y. Y.; Yan, B.; Xue, L. L.; Li, Y.; Luo, X. Y.; Ji, P. *Lipids Health Dis.* **2019**, 18.
(40) Chan, J. W.; Taylor, D. S.; Zwerdling, T.; Lane, S. M.; Ihara, K.; Huser, T. *Biophys. J.* **2006**, *90*, 648−656.
(41) Krafft, C.; Neudert, L.; Simat, T.; Salzer, R. *Spectrochim. Acta. A Mol. Biomol. Spectrosc.* **2005**, *61*, 1529−1535.
(42) Malini, R.; Venkatakrishna, K.; Kurien, J.; Pai, K. M.; Rao, L.; Kartha, V. B.; Krishna, C. M. *Biopolymers* **2006**, *81*, 179−193.
(43) Silveira, L.; Borges, R. D. F.; Navarro, R. S.; Giana, H. E.; Zangaro, R. A.; Pacheco, M. T. T.; Fernandes, A. B. *Laser. Med. Sci.* **2017**, *32*, 787−795.
(44) Luo, H.; Weaver, M. J. *Langmuir* **1999**, *15*, 8743−8749.
(45) van Wilderen, L. J. G. W.; Kern-Michler, D.; Muller-Werkmeister, H. M.; Bredenbeck, J. *Phys. Chem. Chem. Phys.* **2017**, *19*, 9676−9678.
(46) Druml, W.; Roth, E.; Lenz, K.; Lochs, H.; Kopsa, H. *Kidney Int.* **1989**, *36*, S282−S286.
(47) Kopple, J. D. *J. Nutr.* **2007**, *137*, 1586s−1590s.
(48) Bennett, M.; Dent, C. L.; Ma, Q.; Dastrala, S.; Grenier, F.; Workman, R.; Syed, H.; Ali, S.; Barasch, J.; Devarajan, P. *Clin. J. Am. Soc. Nephro.* **2008**, *3*, 665−673.
(49) Devarajan, P. *Expert. Opin. Med. Diagn.* **2008**, *2*, 387−398.
(50) Zhang, Z. H.; Lu, B. L.; Sheng, X. Y.; Jin, N. *Am. J. Kidney. Dis.* **2011**, *58*, 356−365.


https://doi.org/10.1021/acs.analchem.2c03634
*Anal. Chem.* 2022, 94, 17477−17484